JOURNAL OF CATALYSIS 114, 46–52 (1988)

The Tunneling Action of Group VIII Metal Particles in Catalyzed Graphite Hydrogenation

PETER J. GOETHEL AND RALPH T. YANG

Department of Chemical Engineering, State University of New York, Buffalo, New York 14260

Received March 29, 1988

A new catalyst action in catalyzed graphite hydrogenation, termed tunneling, is observed and studied for Pt, Ni, and Ru. The metal particles undergo tunneling in the *a* direction of graphite (parallel to the basal plane), gasifying carbon. The linear speed of tunneling is independent of particle size. The sequential steps in the reaction are C–C bond breakage and dissolution of carbon into the metal at the leading-edge carbon–metal interface, diffusion of carbon in metal, and reaction between C and H on metal surface. The last step is rate limiting, and is a common step for deep-layer channeling, monolayer channeling, as well as the methanation reaction. Both tunneling and monolayer channeling actions are at least as important as deep-layer channeling in the overall rate for graphite hydrogenation.

INTRODUCTION

The graphite hydrogenation reaction (producing CH_4) catalyzed by various group VIII metals has been the subject of many studies [e.g., (*1–10*)]. The studies on bulk powders employing thermogravimetric analysis (TGA) or evolved gas analysis do not reveal the catalyst actions by the metal particles on carbon surfaces. A large number of microscopic investigations using optical and electron microscopic techniques have been undertaken to study the deep-layer channeling action of the catalysts (*1, 4–7, 11*). A typical SEM picture illustrating deep-layer channeling is given in Fig. 1. Another important catalyst action, termed monolayer channeling, has been observed and studied in our laboratory recently (*12–14*). The mechanistic steps involved in monolayer channeling are similar to those in deep-layer channeling. A comparison of the contributions made to the overall reaction rate by deep-layer channeling and by monolayer channeling indicates that monolayer channeling is at least as important as, and likely far more important than, deep-layer channeling (*14*). However, monolayer channeling can be observed only by the gold-decoration technique (*15*), and is not visible in controlled-atmosphere TEM (CAEM) studies (*1, 5–7, 10*). For this reason monolayer-channeling particles have been thought (mistakenly) to be undergoing random particle motion on the graphite basal plane by previous investigators using CAEM.

Still another important catalyst action, termed tunneling, has been observed in our laboratory, and the results are presented in this report. In the metal (or metal oxide)-catalyzed graphite–oxygen reaction, particles have been found to move along the *c* axis (normal to the basal or layer plane) of graphite into the bulk of the graphite, and the action has been termed pitting. Pitting does not occur in the catalyzed hydrogenation reaction. The question to be addressed is then whether the catalyst particles can move along an *a* axis (parallel to the layer plane) of graphite and gasify carbon. This catalyst action, termed tunneling, has indeed been observed and studied for group VIII metals (Ni, Pt, and Ru) in the C–H_2 reaction.

EXPERIMENTAL

The graphite used in the study was Ticonderoga graphite. It was used because of its large single-crystal sizes as well as the

0021-9517/88 $3.00

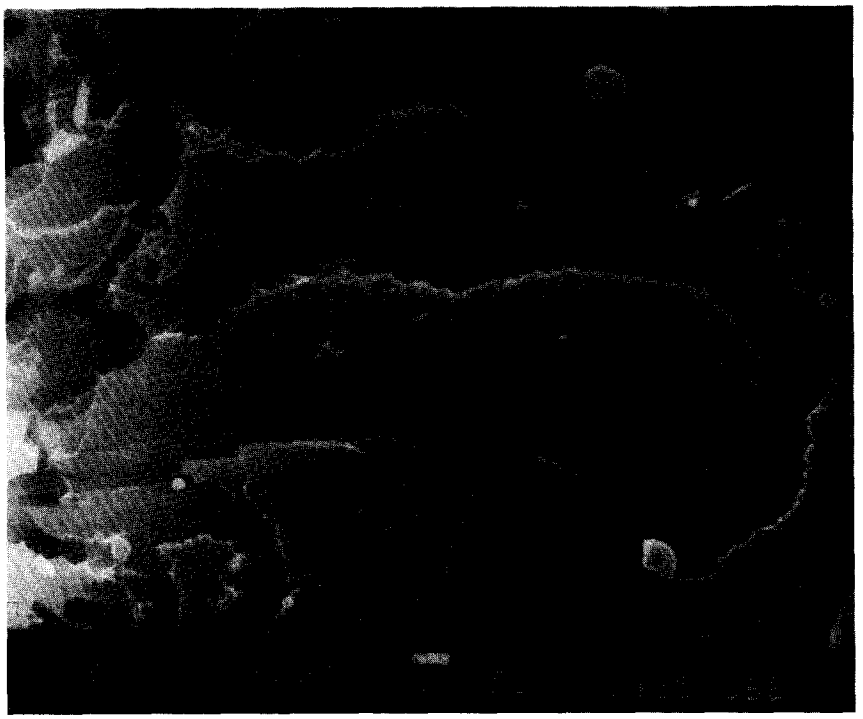

FIG. 1. SEM picutre of a deep-channeling platinum particle on the basal plane of graphite after reaction with 1 atm H_2 at 1050°C for 7 h and 17 min.

ease of its cleavage. The metal catalyst powder was placed in contact with the edges of the graphite crystal. The mixed sample was supported on a sapphire plate which was placed in a combustion boat. The combustion boat was then placed in a quartz reaction tube for the hydrogenation reaction. The gases used were hydrogen (99.999% minimum purity) and helium (99.999% minimum purity). Gases were further purified by passage through long-path beds packed with 13X and 4A zeolite, both held at liquid nitrogen temperature. Other experimental details are given elsewhere (*12, 15*).

Figure 2 is an illustration of the three experimental steps involved in preparing the sample for viewing of tunnels. Figure 2A shows the initial application of the catalyst particle in contact with the graphite crystal edge. Figure 2B shows the sample directly after reaction with hydrogen, and Fig. 2C is a view of the halves of the graphite crystal after being cleaved open. Mirror images are seen on the open faces which are the cleaved tunnel halves with the catalyst particle remaining on one face. An Amray

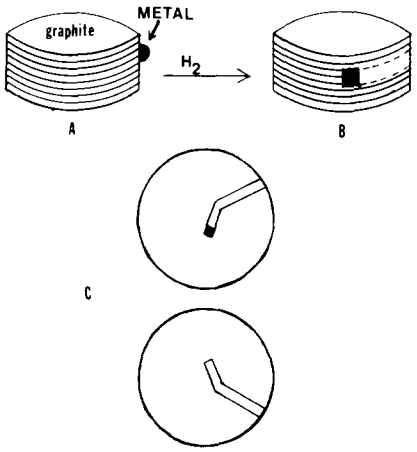

FIG. 2. Schematic of experimental procedure for studying catalyst undergoing tunneling action in graphite hydrogenation. The graphite crystal is cleaved open after reaction to reveal halves of the tunnel.

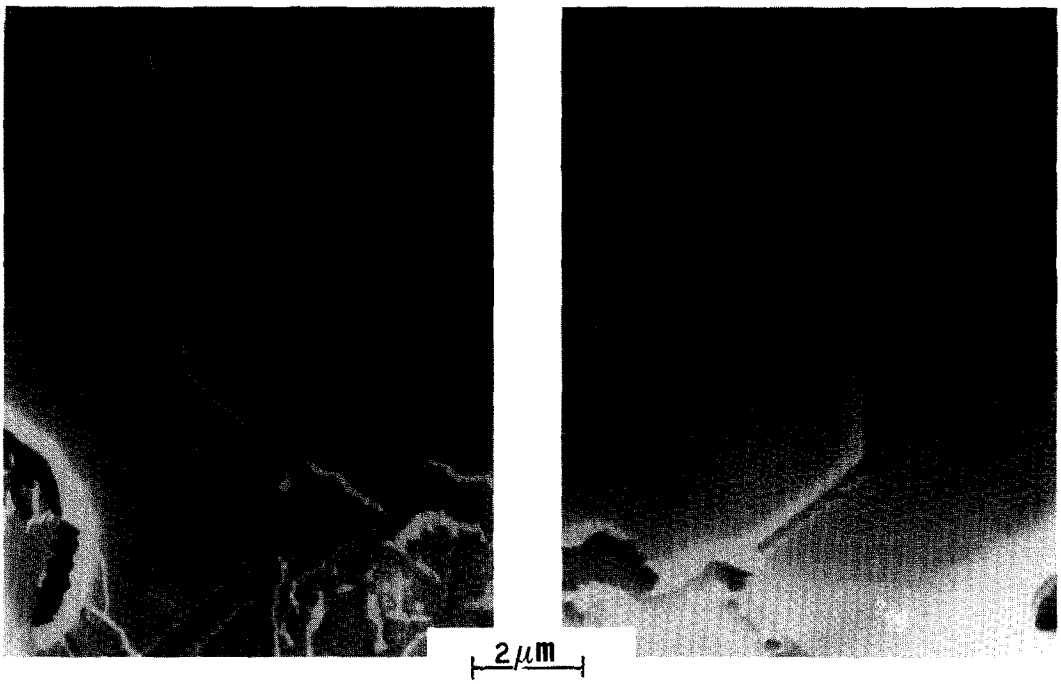

FIG. 3. SEM of cleaved tunnel which was formed by platinum particle after reaction of graphite/Pt with 1 atm H_2 at 1000°C for 1045 min.

1000A scanning electron microscope was used to analyze the cleaved tunnel dimensions. From these data the catalyzed reaction rates were calculated.

The particle was assumed to start tunneling when the hydrogen atmosphere was introduced into the preheated system. Experiments were performed with the graphite/metal samples heated in helium for several hours at the reaction temperature and no reaction was observed. An assumption made in measuring rate data was that the tunneling speeds were not a function of time, i.e., the catalyst was assumed not to deactivate. The deep-layer (*1, 5–7*) and monolayer (*12–14*) channeling particles do not deactivate during the reaction at the temperatures studied; thus deactivation of the catalyst during the tunneling action is highly unlikely.

RESULTS AND DISCUSSION

The catalysts studied for the C–H_2 reaction were platinum, nickel, and ruthenium. The particle sizes studied were below 1 μm. Typical SEM pictures of the cleaved tunnels created by these three catalysts (following the procedure shown in Fig. 2) are shown, respectively, for the three catalysts, in Figs. 3, 4, and 5. Particle sizes varying from 0.1 to 1.0 μm were viewed in the tunneling mode of catalysts. For a particular size of particles the tunnel lengths were measured and the longest tunnel measured was used in the rate calculation. Shorter tunnels originate from particle movement (channeling) along the graphite crystal edges prior to initiation of tunneling action. The rate data as calculated are therefore minimum gasification rates. To within an experimental error of ±5%, all particles were found to tunnel at the same speed independent of the particle size. This result is in contrast to monolayer and deep-layer channeling. In monolayer and deep-layer channeling, the channeling speed is proportional to the particle size (for sizes below 1 μm) (*6, 7, 10, 12–14*). However,

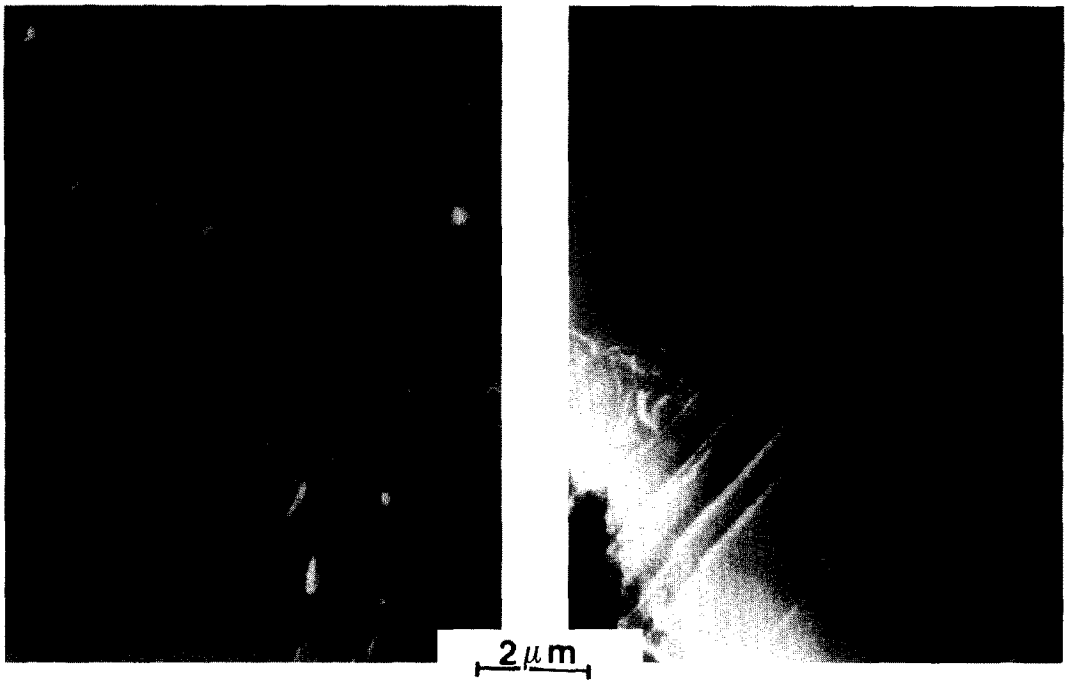

FIG. 4. SEM of cleaved tunnels which were formed by Ni particles after reaction of graphite/Ni with 1 atm H_2 at 900°C for 153 min.

FIG. 5. SEM of cleaved tunnel which was formed by Ru particle after reaction of graphite/Ru with 1 atm H_2 at 950°C for 225 min.

these two contrasting behaviors are expected if the surface reaction at the metal–hydrogen interface is the rate-limiting step in both catalyst actions.

Studies on monolayer channeling (*12–14*) and deep-layer channeling (*5–7*) have established the following sequential mechanistic steps for the channeling action: breakage of C–C bonds at the metal–carbon edge interface and dissolution of carbon into the metal, diffusion of carbon through the metal, and reaction of carbon with chemisorbed hydrogen to form methane on the metal surface. The driving forces for the particle movement are the adhesion forces between metal and edge carbon. The same mechanistic steps and driving forces for particle movement are also pertinent to the tunneling action based on the speed–size relationship and the rate comparisons to be given below. A further result from the channeling study is that the surface reaction between carbon and chemisorbed hydrogen is the rate-limiting step. The observation in this study that particles of all sizes travel at the same speed is an indication that surface reaction may also be the rate-limiting step for tunneling. This is because the surface area of the particle exposed to hydrogen is proportional to the diameter squared. The volume of carbon removed per unit length of tunnel is also proportional to the diameter squared. Thus, no particle diameter dependence is expected for a surface reaction-limited process. If the reaction was diffusion (carbon in metal) limited, smaller particles should tunnel at higher speeds; however, this behavior was not observed for particles less than 1 μm in diameter.

Table 1 shows the rates of tunneling compared to the rates of monolayer channeling based on per unit metal surface area. The tunneling rates are consistently higher by approximately one order of magnitude for all catalysts studied. A possible reason for these consistently higher rates for tunneling is that, inasmuch as both tunneling and channeling particles are faceted, the gas–metal interfaces on the tunneling particles may consist of more energetic and active faces, e.g., higher-index faces. Another possible contributing factor to the higher rates would involve the C–C bond breakage step (at the carbon–metal interface) in the overall rate. Although surface reaction is clearly the slowest step, the C–C bond breakage step may have also intruded into the overall rate. The multilayer graphite edge in tunneling would provide a larger carbon source and hence a higher overall rate for tunneling than for monolayer channeling. A more interesting explanation involves the cooperative effect. The cooperative effect refers to the orders-of-magnitude higher rates for carbon gasification on a multilayer graphite edge than on a monolayer graphite edge. This effect has been observed for graphite gasification by O_2 (*17, 18*) and by H_2O (*19*). Although not understood, the cooperative effect manifests that a lower energy is required for breaking the C–C bonds on a multilayer edge than on a monolayer edge. And such an effect could result in the observed one-order-of-magnitude higher rate for tunneling compared to monolayer channeling. The mechanism for C–C bond breakage is also not understood, but the involvement of electron transfer is probable (*2, 20*).

Surface reaction between carbon (from dissociation of CO) and chemisorbed hydrogen has been thought to be the rate-limiting step for the methanation reaction. Table 2 shows a rate comparison of methanation with the three modes of catalyst

TABLE 1

Comparison of Gasification Rates (Based on Gas–Metal Interface) for Monolayer Channeling and Tunneling

Catalyst	Temperature (°C)	Monolayer channeling (C atoms/cm^2/s)	Tunneling (C atoms/cm^2/s)
Pt	1000	1.0×10^{14}	3.3×10^{15}
Ni	900	1.01×10^{15}	1.3×10^{16}
Ru	950	1.7×10^{15}	1.1×10^{16}

TABLE 2

Comparison of Rates for Methane Production by Three Catalytic Actions in Carbon Hydrogenation and Methanation

Mode of Action	Pt	Ni	Ru
Monolayer channeling (900°C) (C atoms/cm^2 metal/s)	1.49×10^{13}	1.01×10^{15}	1.15×10^{15}
Deep-layer channeling[a] (975°C) (nm/s)	0.1	3.2	17.8
Tunneling (C atoms/cm^2 metal/s)	3.27×10^{15} (1000°C)	1.28×10^{16} (900°C)	1.06×10^{16} (950°C)
Methanation[b] (350°C)	NA[c]	9.7×10^{14}	8.0×10^{14}

[a] Results by Baker *et al.* (*1, 6, 7, 10*); channel depths unknown.
[b] Results by Goodman *et al.* (*16*).
[c] Methanol is the predominant product.

action in carbon hydrogenation. For deep-layer channeling (*1, 5–7, 10*) the Ru-catalyzed gasification rate is substantially higher than the Ni-catalyzed rate. This conflicts with the rate comparison in monolayer channeling and in tunneling where the rates are nearly equal for Ni and Ru. The rates of methanation at 350°C are also (*16*) of the same order of magnitude for Ni and Ru catalysts.

Figure 6 illustrates the mechanistic steps involved in the tunneling action. Surface reaction between carbon and hydrogen atoms is clearly the slowest step. The C–C bond breakage step may have an effect on the overall rate. The tunneling of Ru (Fig. 5) exhibits a random direction (unlike Ni and Pt which take well-defined directions). This may be related to the fact that Ru has a much higher Tammann temperature than Ni and Pt. However, the fact that Ru undergoes tunneling at all was unexpected, because the solubility of carbon in Ru was thought to be nil. The vigorous tunneling action by Ru requires large fluxes of carbon through the metal, which in turn requires a reasonably high solubility. The solubility of carbon in Ru was measured by a simple and accurate TGA technique (details to be published elsewhere). The C/Ru solubility at 850°C is 0.102 at.%, a reasonably high solubility.

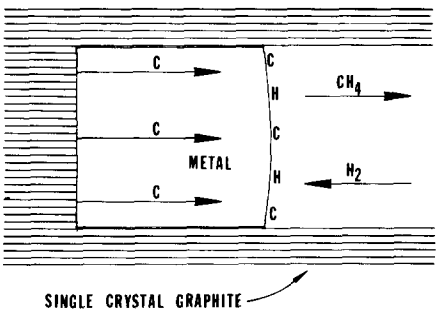

FIG. 6. Schematic representation of the mechanism for tunneling in the metal-catalyzed C–H_2 reaction. The adhesion forces at the metal–graphite interface provide the driving forces for particle movement.

The relative contribution by tunneling to the overall C–H_2 reaction compared to that by deep-layer channeling can be estimated. An estimate may be made by considering the reaction between a mixture of catalyst powder and small graphite crystals. Deep-layer channeling is undertaken by metal particles in contact with the graphite edges near the exterior basal planes of the crystal. Tunneling takes place by particles on the large-edge surface area. By considering 0.25-μm metal particles mixed with 100-μm graphite disks (with equal diameter and thickness), the ratio of the number of tunnel initiation sites to the number of deep-layer channel initiation sites is 200 to 1. Since both catalytic actions are nearly limited by the surface reaction, the rates for the two actions are equal for particles of the same size. The above estimate illustrates the relative importance of tunneling to the overall reaction. The relative importance of monolayer channeling to deep-layer channeling has been discussed elsewhere (*14*).

ACKNOWLEDGMENT

This work was supported by the National Science Foundation under Grant CBT-8703677.

REFERENCES

1. Baker, R. T. K., Lund, C. R. F., and Chludzinski, J. J., Jr., *J. Catal.* **87,** 255 (1984).
2. Holstein, W. L., and Boudart, M., *J. Catal.* **72,** 328 (1981).
3. (a) Tomita, A., and Tamai, Y., *J. Catal.* **72,** 293

(1972); (b) Tomita, A., Sato, N., and Tamai, Y., *Carbon* **12,** 143 (1974).
4. McKee, D. W., *in* "Chemistry and Physics of Carbon" (P. L. Walker, Jr., and P. A. Thrower, Eds.), Vol. 16, p. 1. Dekker, New York, 1981.
5. Keep, C. W., Terry, S., and Wells, M., *J. Catal.* **66,** 451 (1980).
6. Baker, R. T. K., and Chludzinski, J. J., Jr., *J. Phys. Chem.* **90,** 4730 (1986).
7. Baker, R. T. K., Sherwood, R. D., and Derouane, E. G., *J. Catal.* **75,** 382 (1982).
8. Grigor'ev, A. P., Lifshits, S. K., and Shamaev, P. P., *Kinet. Catal.* **18,** 948 (1977).
9. Rewick, R. T., Wentrcek, P. R., and Wise, H., *Fuel* **53,** 274 (1974).
10. Baker, R. T. K., Sherwood, R. D., and Dumesic, J. A., *J. Catal.* **66,** 56 (1980).
11. Hennig, G. R., *J. Inorg. Nucl. Chem.* **24,** 1129 (1962).
12. Goethel, P. J., and Yang, R. T., *J. Catal.* **101,** 342 (1986).
13. Goethel, P. J., and Yang, R. T., *J. Catal.* **108,** 356 (1987).
14. Goethel, P. J., and Yang, R. T., *J. Catal.* **111,** 220 (1988).
15. Yang, R. T., *in* "Chemistry and Physics of Carbon" (P. A. Thrower, Ed.), Vol. 19, p. 163. Dekker, New York, 1984.
16. Goodman, D. W., Kelley, R. D., Madey, T. E., and White, J. M., *J. Catal.* **64,** 479 (1980).
17. Evans, E. L., Griffiths, R. J. M., and Thomas, J. M., *Science* **171,** 174 (1971).
18. Wong, C., and Yang, R. T., *Carbon* **20,** 253 (1982).
19. Yang, R. T., and Yang, K. L., *Carbon* **23,** 537 (1985).
20. Long, F. J., and Sykes, K. W., *J. Chim. Phys.* **47,** 361 (1950).